Inter*net* Electronic Journal of Molecular Design

Structural Contributions for Thermostability of a New Endo–1,4–β–xylanase from the Fungus *Humicola grisea*

Sonia M. De Freitas,[1] Werner L. Treptow,[1,2,4] Fabricia P. De Faria,[3] Maristela De O. Azevedo,[4] and Bernard Maigret[2,5]

[1] Universidade de Brasília (UnB); Departamento de Biologia Celular; Laboratório de Biofísica; Campus Universitário Darcy Ribeiro – Asa Norte; 70910–900; Brasília – DF, Brazil
[2] Universidade de Brasília, Instituto de Química, Laboratório de Modelagem Molecular, Campus Universitário Darcy Ribeiro – Asa Norte – 70910–900, Brasília, DF – Brazil
[3] Universidade Federal de Goiás, Departamento de Ciências Fisiológicas, Lab. Biologia Molecular, Goiânia, GO, Brazil
[4] Universidade de Brasília, Departamento de Biologia Celular, Laboratório de Biologia Molecular, Brasília, DF, Brazil
[5] Laboratory of Theoretical Chemistry, UMR 7565, H. Poincare University, Nancy, France

Citation of the article:
S. M. De Freitas, W. L. Treptow, F. P. De Faria, M. De O. Azevedo, and B. Maigret, Structural Contributions for Thermostability of a New Endo–1,4–β–xylanase from the Fungus *Humicola grisea*, *Internet Electron. J. Mol. Des.* **2003**, *2*, 835–851, http://www.biochempress.com.

Structural Contributions for Thermostability of a New Endo–1,4–β–xylanase from the Fungus *Humicola grisea*[#]

Sonia M. De Freitas,[1,][*] Werner L. Treptow,[1,2,4] Fabricia P. De Faria,[3] Maristela De O. Azevedo,[4] and Bernard Maigret[2,5]

[1] Universidade de Brasília (UnB); Departamento de Biologia Celular; Laboratório de Biofísica; Campus Universitário Darcy Ribeiro – Asa Norte; 70910–900; Brasília – DF, Brazil
[2] Universidade de Brasília, Instituto de Química, Laboratório de Modelagem Molecular, Campus Universitário Darcy Ribeiro – Asa Norte – 70910–900, Brasília, DF – Brazil
[3] Universidade Federal de Goiás, Departamento de Ciências Fisiológicas, Lab. Biologia Molecular, Goiânia, GO, Brazil
[4] Universidade de Brasília, Departamento de Biologia Celular, Laboratório de Biologia Molecular, Brasília, DF, Brazil
[5] Laboratory of Theoretical Chemistry, UMR 7565, H. Poincare University, Nancy, France

Abstract

The *Humicola grisea* var. *thermoidea* is known as a good producer of hydrolytic enzymes. The *H. grisea* endo–1,4–β–xylanase gene (*xyn2*) was isolated and its sequence was translated into a predicted protein coding for a xylanase of 23 kDa. A structural model of *H. grisea* endo–1,4–β–xylanase (XYN2) was built by homology modeling based on the database search results of related proteins, belonging to Glycoside Hydrolase Family 11 (GH11). The inactive/active conformation transition of the XYN2 model active site is pH sensitive as revealed by independent molecular dynamics simulations at different pH. The active conformation exhibits the common structural β–sheet twisted architecture of the GH11. The active site is formed by a large cleft containing the catalytic residues (E84 and E175), and is stabilized by hydrogen bond network involving the Q134, Y75, Y88, W77, and Y169. Additionally, the structural properties described by the model explain the observed thermostability of the XYN2 protein. According to our results, the thermostability of XYN2 protein, compared to mesophilic xylanases, can be explained by an additional electrostatic network and extra aromatic exposed residues.

Keywords. *Humicola grisea*; molecular modeling; structural stability; xylanases; glycoside hydrolase; protein structure.

1 INTRODUCTION

Xylan is a major constituent of hemicellulose present in the plant cell wall, comprising up to 39% of the dry weight of terrestrial plants. This polysaccharide is composed of β–1,4–linked xylopyranose units, with substitutions generally occurring at the C–2 or C–3 atoms [1]. Endo–1,4–β–xylanases and β–xylosidases act in the nature by depolymerizing xylan molecules into monomeric xylose units that are used by bacterial and fungal populations as a primary carbon source [2,3]. The mechanism of endo–1,4–β–xylanases involves acid catalysis. Two critical glutamate residues, acting as a proton donor and a nucleophile/base [5], hydrolyze the xylan in anomeric xylopyranose units. Endo–1,4–β–xylanases are classified as glycoside hydrolases belonging to GH10 and GH11 families, respectively (http://afmb.cnrs–mrs.fr/ ~cazy/CAZY/index.html). GH10 xylanases have a molecular mass of approximately 35 kDa, while GH11 xylanases have a molecular mass of about 20 kDa and can have either a high or low pI [4].

All structures of xylanases belonging to the GH11 family are similar and have a common fold for the catalytic domain. The overall fold has been compared to the shape of a right hand [6], with the fingers localized at the bottom of the palm, at the right hand side, and the thumb localized at the top of the molecule. The structure of xylanases consists of a single domain composed of 14 twisted antiparallel β–sheets and one α–helix positioned at the top of the thumb region. The arrangement of the structural β–sheets forms a long cleft containing the two catalytic glutamate residues and the solvent–exposed aromatic residues [6]. Xylanases of GH11 family contain a large number of aromatic residues, positioned at the active cleft to bind substrate through stacking and hydrogen bond interactions. Solvent exposed aromatic residues out of the active cleft are arranged as sticky patches inducing oligomerization and contributing to the stability of thermophilic proteins [7].

Interest in xylanases has increased in the last decade due to their biotechnological applications. Xylanases have been used in the paper industry for bleaching paper pulps [8,9], in bioconversion of plant biomass and in plant fertilizers or chemical for food industries [10]. For successful selection of xylanases suitable for specific industrial applications it is important to characterize xylan–degrading enzymes isolated from different sources. The occurrence of multiple forms of xylanases has been documented for many microbial systems suggesting that this diversity serves as a mean to achieve effective hydrolysis of diverse xylan substrates [3].

The thermophilic fungus *H. grisea* var. *thermoidea* isolated from Brazilian soil has proved to be a good source of xylanolytic enzymes and β–D–xylosidases [11,12]. Two xylan–hydrolyzing enzymes of molecular mass of 20 and 23 kDa were purified from *H. grisea*. In addition, isolation of a *H. grisea* gene encoding a putative xylanase of GH10 family with a cellulose–binding domain and a predicted molecular mass of 47 kDa has been reported [13].

The present study describes the isolation of the xylanase (*xyn2*) gene of *H. grisea*. XYN2 was

previously characterized as a thermostable protein [12]. An atomistic model of XYN2 was obtained by molecular modeling and relaxed by molecular dynamics in order to investigate molecular properties implicated in the observed thermal stability. Structural features obtained from MD trajectory were compared to known thermophilic and mesophilic xylanases [14]. Our study demonstrates that the thermal stability of XYN2 protein compared to mesophilic xylanases could be explained by the additional electrostatic network and aromatic exposed residues.

2 MATERIALS AND METHODS

2.1 Microbial Strains and Culture Conditions

The wild–type strain of the fungus *H. grisea* var. thermoidea [15] was grown on 4% (w/v) of meal baby food (Quaker) plates at 42 °C until conidiation and maintained at 4 °C. For liquid cultures, 1×10^6 spores mL^{-1} were inoculated in minimal medium (MM) [16] supplemented with ball–milled straw (BMS) prepared from crude material [10]. After 48 h of incubation the *H. grisea* mycelium was harvested and used for nucleic acid extraction.

2.2 Selection of *xyn2* Gene from *H. grisea*

The *xyn2* gene sequence from *H. grisea* was obtained by screening a previously prepared cDNA library, using total RNA [17] from fungal cells grown under induction by 1% BMS. For the construction of recombinant bacteriophages, Strategene lambda Zap II system and Gigapack kits were used. A homologous probe (xyn1/2) was obtained by PCR, using the oligonucleotide primers Hxyn1 and Hxyn2, designed according to conserved amino acid residues and nucleotide sequences, and genomic DNA [18] (Table 1). The PCR steps consisted of denaturation at 94 °C for 1 min, annealing at 45 °C for 1 min, and primer extension at 72 °C for 90 sec with 35 cycles.

Table 1. Oligonucleotide primers used in this work.

Oligonucleotide primer	Sequence
Hxyl1	5'ATGGTCTCG(C/T)TCAA(G/A)TCT(G/C)T 3'
Hxyl2	5'AG(T/A)ACT(A/G)(G/C)CTGGA(G/C)GTCCGG 3'

The amplified DNA fragment was sub–cloned onto PGEM–Tvector (Promega) and sequenced. For e screening, recombinant plaques were blotted onto nylon membranes (Amersham) and hybridized with the xyn1/2 probe ^{32}P–labeled (10^9 cpm μg^{-1}) under low stringency [19]. Positive clones were purified, amplified and converted into the pBluescriptSK(–) form as described by Stratagene. Plasmidial DNA was analyzed by Southern–blotting and sequenced. Computer analysis was carried out with the Wisconsin Package (Genetics Computer Group, WI, USA). The obtained *xyn2* sequence from *H. grisea* was submitted to the GenBank nucleotide sequence database (AF155594).

2.3 Domain Analyses and Sequence Alignment

The XYN2 sequence was obtained from cDNA and consists of a single chain of 208 amino acids length. The domain organization and the relationship of XYN2 with other related domains of protein families were determined using the PRODOM website (http://www.toulouse.inra.fr/ prodom/). The classification of the xylanase protein family was checked using the PROSITE (http://www.expasy.ch/) gateway. The secondary structure predictions, used as additional information to check the sequence alignments, were obtained from the Secondary Prediction Consensus package Network Protein Sequence – NPS (http://pbil.ibcp.fr/).

An extensive sequence alignment search was performed against the Protein Data Bank (PDB) database using the Blast and FASTA software [20,21]. The suitable templates were selected according to the following experimental data (*i*) the GH11 domains organization and the specific localization of the active site; (*ii*) the primary structure identity scores; (*iii*) the conserved residues within the secondary elements.

2.4 Models Building

The whole molecular modeling procedure was done using Insight II from MSI (MSI, San Diego, 1991). The sequence alignment was inspected considering that the secondary structure is typically conserved between homologous proteins and the insertions and/or deletions in these regions of the sequence alignment must be avoided. The amino acids coordinates of the template presenting the highest primary identity within the secondary structural elements concerning the XYN2 sequence were assigned. Additionally, polypeptide loops were randomly generated for gap regions.

The energy refinement of the XYN2 model was done using molecular mechanics capabilities and the consistent valence force field (CVFF). Steepest descents (SD) and conjugate gradients (CG) algorithms were used successively in two minimization steps. In the first one, all the backbone atoms were constrained and a short energy minimization (EM), using SD algorithm (100 interactions), followed by a long one using CG steps (1,000 interactions) were carried out. In the next steps, all constrains were removed following the same parameters for minimization. A distance–dependent dielectric constant was used in order to avoid the overestimation of electrostatic effects. The minimized model was submitted to two independently molecular dynamics (MD) simulations, starting from the same structure with different velocities in order to check the ergodic hypothesis. Each of the MD simulations consisted of 100 ps at 300K with a 10 Å cutoff. In almost of described xylanase proteins the optimum pH is near the pI value [22]. Therefore, the MD simulations were performed at pH 8.0, considering the predicted pI 8.1 of XYN2 (http://www.expasy/ch).

The final conformation of each MD trajectory was submitted to energy minimization using SD and CG as described above. The minimized models were discriminated according to the following

seven criteria: (*i*) the distances between E84 and E174, defined by alpha carbon atom distances and carboxylic oxygen atom distances, during the MD trajectory; (*ii*) the secondary RMSD (root mean square deviation) between the XYN2 model and the selected templates, (*iii*) the hydrogen bond network of the active site of the 'Thumb' region and of the largely conserved residues in GH11 family; (*iv*) the relative solvent accessibility profile and structural accessibility compared with all chosen templates [23]; (*v*) the secondary structural arrangements and (*vi*) the stereo–chemical analysis of the XYN2 model performed with the PROCHECK program [24].

3 RESULTS AND DISCUSSION

3.1 Isolation of the *H. grisea xyn2* Gene

The oligonucleotide primers Hxyn1 and Hxyn2 amplified a genomic DNA fragment of *H. grisea* of 0.6 kb converted into a homologous probe for the library screening (Table 1). The recombinant clone Hxyn2–1.8, harboring the longest insert (1.0 kb), was sequenced for both strands. This fragment shares high similarity with xylanase genes from *H. insolens* [25], and *Aspergillus niger* [26]. Figure 1 shows the nucleotide sequence of *H. grisea xyn2* and its deduced amino acid sequence. The *xyn2* nucleotide sequence displays an open reading frame of 681 bp interrupted by two introns. The presence of introns indicates contamination of the RNA preparation with fragments of genomic DNA since DNAse treatment was omitted during the construction of cDNA library. The resulting sequence showed high homology with GH11 family and therefore was designated as *H. grisea xyn2* genomic sequence.

3.2 Analysis of the *H. grisea xyn2* Gene and XYN2 Amino Acid Sequence

The entire nucleotide sequence of DNA isolated from Hyn2–1.8 containing the *xyn2* gene comprises 1002 nucleotides (nt), including 107 nt from the 5' upstream region and 79 nt from the 3' untranslated region. The occurrence and location of introns was confirmed by comparison with DNA sequences from the corresponding cDNA obtained by RT–PCR (data not shown). The intron/exon junction followed the GT–AG rule and the lengths of the introns (74 and 57 bp) are in accordance with other filamentous fungal introns [27]. The 5'–noncoding region of *H. grisea xyn2* shows at the position –105, relative to the putative start codon, a TATA box–like sequence. At –22 was localized a 6 bp site with a consensus sequence for binding the CREA catabolitic repressor in *Aspergillus nidulans* and *Trichoderma reesei* CRE1 (5'–SYGGRG–3'; S=G or C, Y=C or T, R=G or A) [28]. The highest sequence similarities were found for *H. insolens* XYN1 (97.8%) [25], *Cochliobolus carbonum* XYL1 (63.5%) [29], *Emericella nidulans* XYN1 (62.2%), *E. nidulans* XYN2 (57.7%) [30], *A. niger* XYN2 (57.2%) [26], *Aspergillus awamori* XYNB (56.3%) [31], and *T. reesei* XYNII (54.7%) [32]. The *H. grisea xyn2* gene encodes a putative protein of 227 amino acids residues. The alignment with fungal xylanases and the hydrophobic profile of the deduced

protein suggest that the precursor of XYN2 has an amino terminal signal sequence of 19 amino acids (Figure 1) and the mature enzyme is composed of 208 amino acids with a molecular mass of 23 kDa. Sequence analysis of XYN2 also revealed a putative target for N–glycosylation on N10 of the mature protein (N–X–S/T, where X is not P) [33].

```
-107            AATATAAAAGGCTGATGGAGGAACGTCAAGGTGATCTTGTCGACTTC
 -61   TCGCCACAACCGtCGTGCCTCGTCACTTGCCTACGATCCTCCAGCAACTCACAGTTCACC
   1   ATGGTCTCGATCAAGTCTGTCCTCGCAGCCGCCACGGCTGTGAGCTCTGCTCTTGCTGCC
       M  V  S  I  K  S  V  L  A  A  A  T  A  V  S  S  A  L  A      20
  61   CCCTTTGACTTCGTTCCTCGGGACAACTCGACGGCCCTTCAGGCTCGCCAGGTGACCCCC
       P  F  D  F  V  P  R  D  N  S  T  A  L  Q  A  R  Q  V  T  P   40
 121   AACGCTGAGGGCTGGCACAACGGCTACTTCTACTCGTGGTGGTCCGACGGCGGAGGCCAG
       N  A  E  G  W  H  N  G  Y  F  Y  S  W  W  S  D  G  G  G  Q   60
 181   GTTCAGTACACGAACCTTGAGGGCAGCCGTTACCAGGTCAGATGGCGTAACACCGGCAAC
       V  Q  Y  T  N  L  E  G  S  R  Y  Q  V  R  W  R  N  T  G  N   80
 241   TTCGTCGGTGGTAAGGGTTGGAACCCGGGAACCGGCCGGTAAGTCTTGTGCCCTTGTTGA
       F  V  G  G  K  G  W  N  P  G  T  G  R                       93
 301   TCAGATTTGCCAGAGAGGCACGTTATGTCCAAGAAATACTGACAGCCTGTAGCACGATC
                                                        T  I        95
 360   AACTACGGTGGTTACTTCAACCCCCAGGGCAACGGCTACCTGGCCGTCTATGGCTGGACC
       N  Y  G  G  Y  F  N  P  Q  G  N  G  Y  L  A  V  Y  G  W  T   115
 420   CGCAACCCGCTCGTCGAGTACTATGTCATCGAGTCGTACGGCACGTACAATCCCGGCAGC
       R  N  P  L  V  E  Y  Y  V  I  E  S  Y  G  T  Y  N  P  G  S   135
 480   CAGGCTCAGTACAAGGGCACATTCTATACCGACGGCGACCAGTATGACATCTTCGTGAGC
       Q  A  Q  Y  K  G  T  F  Y  T  D  G  D  Q  Y  D  I  F  V  S   155
 540   ACCCGCTACAACCAGCCCAGCATCGACGGCACCCGGACGTTCCAGCAATACTGGTCTATC
       T  R  Y  N  Q  P  S  I  D  G  T  R  T  F  Q  Q  Y  W  S  I   175
 600   CGCAAGAACAAGCGTGTCGGTGGCTCGGTCAACATGCAGAACCACTTCAACGCGTGGCAG
       R  K  N  K  R  V  G  G  S  V  N  M  Q  N  H  F  N  A  W  Q   195
 660   CAGCACGGAATGCCGCTCGGCCAGGTAAGTTCACTGCTCGTCGTGTTGTTGGTTTGGCCA
       Q  H  G  M  P  L  G  Q                                       203
 720   ACGTGACTCACACTTCTGCAGCACTACTACCAGATCGTCGCCACCGAGGGTTACCAGAGC
                                  H  Y  Y  Q  I  V  A  T  E  G  Y  Q  S   216
 780   AGTGGCGAGTCCGACATCTATGTCCAGACTCACTAAGCGACGCACCCCGCAAGAAACGG
       S  G  E  S  D  I  Y  V  Q  T  H                              227
 816   AGGTTGCCAAGATGTGATTGTAACTGACTTTTGTCATGCGCTCGTGCCGAATTCC
```

Figure 1. Nucleotide sequence of the *H. grisea xyn2* gene and its deduced protein amino acid sequence. Intron splicing sequences are delimited with underlined letters. Putative TATA box is delimited with a double line dashed box. The putative leader sequence is delimited with a dashed box. The initiation codon ATG and the stop codon TAA are delimited with underlined bold letters.

3.3 Sequence Analyses and Structural Study of GH11 Family

The XYN2 was characterized as a low–molecular weight endo–1,4–β–glycosyl hydrolase (GH11) [22] according to the primary sequence analysis [34]. The primary sequence conservation among members of this family is mainly restricted to the secondary structure regions as revealed by the primary alignment. Therefore, the primary sequence conservation within the characterized domain regions of the GH11 family was used to investigate potential templates in the PDB. According to this procedure a total of 26 structures of the GH11 family were found and seven xylanase proteins were retained as potential templates. These structures were aligned at the primary

level (Figure 2) considering the conserved secondary structure that characterizes the GH11 family fold. Seventeen N–terminal residues of the mature XYN2 sequence enzyme were not observed in any of the retained templates and were not considered for homology modeling. In Figure 2, the residues belonging to the active sites of GH11 family signatures 1 and 2 (colored in red) are well conserved.

```
                                 B2              A2            A3              B3
XYN2 (    1) QVTPNAEGWHNGYFYSWWSDGGGQVQYTNLEGSRYQVRW--RNTGNFVGGK (49   )
 YNA (    2) TTPNSEGWHDGYYYSWWSDGGAQATYTNLEGGTYEISW--GDGGNLVGGK (49   )
 XYN (    1)        ASINYDQNYQTGGQVSYS-PSNTGFSVNW--NTQDDFVVGV (38   )
 BK1 (    2)       AGINYVQNYNGNLGDFTYDESAGTFSMYWEDGVSSDFVVGL (42   )
 PVX ( A1) GTTPNSEGWHDGYYYSWWSDGGGDSTYTNNSGGTYEITW--GNGGNLVGGK (A49  )
AXK1 (    1) YDWVKYTSNASTDYWQNWTDGGGIVNAVNGSGGNYSVNW--SNTGNFVVGK (49   )
ENX1 (    1)  TIQPGTGYNNGYFYSYWNDGHGGVTYTNGPGGQFSVNW--SNSGNFVGGK (48   )
UKR1 (    1)        GINYVQNYNGNLGDFTYDESAGTFSMYWEDGVSSDFVVGL (40   )

                        A5              B5                       B6
XYN2 (   50) GWNPGTG-RTINY-GGYFNPQGNGYLAVYGWTRNPLVEYYVIESYGTYNPG (98   )
 YNA (   50) GWNPGLNARAIHF-EGVYQPNGNSYLAVYGWTRNPLVEYYIVENFGTYDPS (99   )
 XYN (   39) GWTTGSS-APINFGGSFSVNSGTGLLSVYGWSTNPLVEYYIMEDNHNYPA- ( gap )
 BK1 (   43) GWTTGSS-NAITYSAEYSASGSSSYLAVYGWVNYPQAEYYIVEDYGDYNPC (92   )
 PVX ( A50) GWNPGLNARAIHF-TGVYQPNGTSYLAVYGWTRNPLVEYYIVENFGSSNPS (A99  )
AXK1 (   50) GWTTGSPFRTINYNAGVWAPNGNGYLTLYGWTRSPLIEYYVVDSWGTYRP- ( gap )
ENX1 (   49) GWQPGTKNKVINF-SGSYNPNGNSYLSVYGWSRNPLIEYYIVENFGTYNPS (98   )
UKR1 (   41) GWTTGSS-NAITYSAEYSASGSASYLAVYGWVNYPQAEYYIVEDYGDYNPC (90   )

 Cord              B9                  B8    Thumb           B7
XYN2 (   99) SQAQYKGTFYTDGDQYDIFVSTRYNQPSIDGTRT-FQQYWSIR---KNKRV (145  )
 YNA (  100) SGATDLGTVECDGSIYRLGKTTRVNAPSIDGTQT-FDQYWSVR---QDKRT (146  )
 XYN ( gap  )-QGTVKGTVTSDGATYTIWENTRVNEPSIQGTAT-FNQYISVR---NSPRT (133  )
 BK1 (   93) SSATSLGTVVSDGSTYQVCTDTRTVGTSITGTST-FTQYFSVR---ESTRT (139  )
 PVX ( A100) SGSTDLGTVSCDGSTYTLGQSTRYNAPSIDGTQT-FNQYWSVR---QDKRS (A146 )
AXK1 ( gap  )-TGTYKGTVKSDGGTYDIYTTTRYNAPSIDGDRTTFTQYWSVRQSKRPTGS (149  )
ENX1 (   99) TGATKLGEVTSDGSVYDIYRTQRVNEPSIIGTAT-FYQYWSVR---RNHRS (145  )
UKR1 (   91) SSATSLGTVYSDGSTYQVCTDTRTNEPSITGTST-FTQYFSVR---ESTRT (137  )

                  A6              B4               A4
XYN2 (  146) GGSVNMQNHFNAWQQHGMPLGQHYY-QIVATEGYQSSGESDIYVQTH    (191  )
 YNA (  147) SGTVQTGCHFDAWARAGLNVNGDHYYQIVATEGYFSSGYARITVADVG   (194  )
 XYN (  134) SGTVTVQNHFNAWASLGLHLGQMNY-QVVAVEGWGGSGSASQSVSN     (178  )
 BK1 (  140) SGTVTVANHFNFWAQHGFGNSDFNY-QVMAVEAWSGAGSASVTIS      (183  )
 PVX ( A147) SGTVQTGCHFDAWASAGLNVTGDHYYQIVATEGYFSSGYARITVADVG   (A194 )
AXK1 (  150) NATITFSNHVNAWKSHGMNLGSNWAYQVMATEGYQSSGSSNVTVWGSV   (197  )
ENX1 (  146) SGSVNTANHFNAWAQQGLTLGTMDY-QIVAVEGYFSSGSASITVS      (189  )
UKR1 (  138) SGTVTVANHFNFWAHHGFGNSDFNY-QVVAVEAWSGAGSASVTIS      (181  )
```

Figure 2. Primary sequence alignment of the X–ray crystal coordinates from GH11 family. The residues conserved in all the templates are shown in blue. The two putative catalytic residues (E84 and E175) of the known signature sites 1 (PLV**E**YYVIESY) and 2 (VAT**E**GYQSSGES), respectively, are shown in red. The highest sequence identity scores of about 58% were obtained for 1YNA [35]; 1ENX [44]; 1UKR [36], 1AXK [45]; 1PVX [46]. For 1XYN [44] and 1BK1 [47] the sequence identities were 47% and 39%, respectively. The boxes indicate the region of coordinate assignment by homology modeling. The secondary structure consensus (sheets A and B, helix) and the others regions (Cord and Thumb) of the retained templates are indicated above the alignment.

The hydrophobic sequence profiles of the retained templates are presented in Figure 3. Although all the templates presented similar hydrophobic profiles, the number of charged residues groups of the XYN2 sequence is closest to those of 1YNA and 1PVX. The high content of hydrophobic residues is responsible for the appropriated fold and structural stability for all members of GH11 family [35]. The relative residue solvent accessibility of the templates is shown in Figure 4. All analyzed structures present five characterized buried regions, corresponding to the conserved sequence fragments of the primary level (indicated by arrows). These regions constitute the B3, B5, B6, B7 and B4 β–Sheet strands (Figure 2). The glutamate catalytic residues of the signature sites 1

and 2 belong to the B6 and B4 β–Sheet strands, respectively. These catalytic residues are completely buried, except the 1UKR signature site 2, in which the catalytic residue is partially buried.
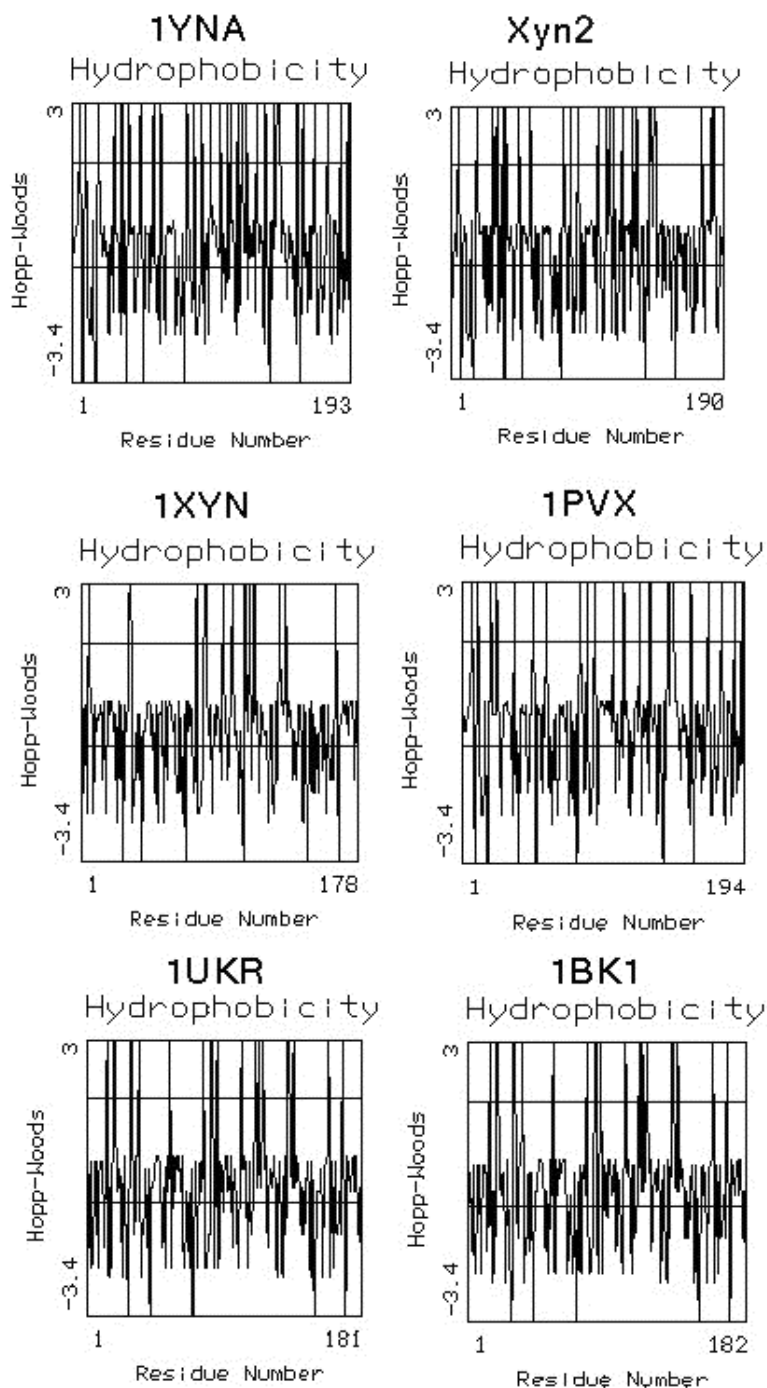
Figure 3. Sequence hydrophobic profiles. The hydrophobic scale used was Hopp–Wood. Due to the number of charged residues, the hydrophobic profile of the XYN2 sequence closely resembles those of 1YNA and 1PVX.

For molecular modeling of the XYN2 protein, among all the selected templates, the 1YNA 3D structure was chosen considering its agreement to the established following criteria: the highest

sequence identity score (Figure 2); the conserved structural arrangement of GH11 family; and the hydrophobic sequence profiles (Figure 3).
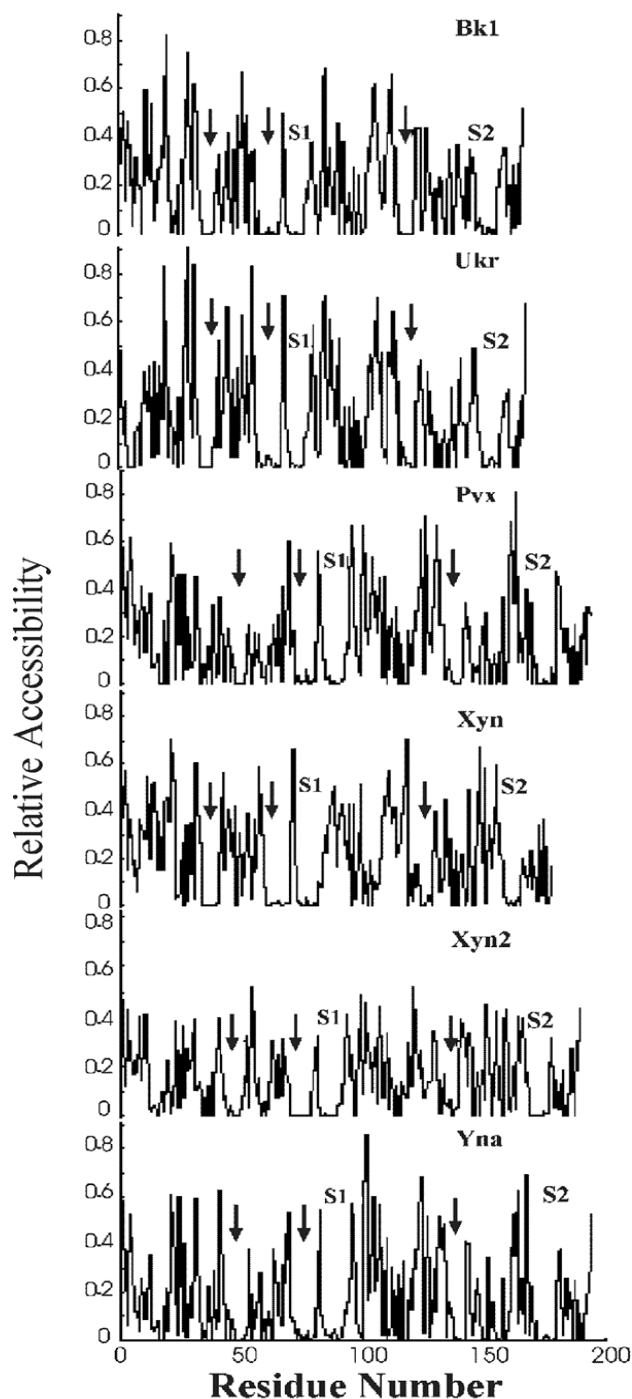
Figure 4. Relative solvent accessibility of xylanase templates. Three buried structural regions corresponding to the B3, B5, and B7 β–strand are depicted by arrow. Additionally, the buried B6 and B4 β–strands are depicted as S1 and S2, respectively. These regions correspond to the active signature sites 1 and 2, respectively. It is worth to note that these regions are highly conserved at the primary level (Figure 2).

3.4 Analysis of Energy Refined Model

Molecular dynamic simulations in vacuum were performed at different pHs in order to analyze the stability of the XYN2 active conformation. As reported in the literature, the catalytic site conformation depends on the pH. For some xylanase proteins activity, the optimum pH is close to the pI value [22]. Indeed, independent MD trajectories at pH 7.0 and 8.0 resulted in different conformation of the active site.

Although the 1ns MD trajectory at pH 7.0 is stable with a small backbone displacement of 0.29 Å (data not shown), the putative active conformation of the active site was not attained (see below). In contrast, at pH 8.0 the putative active conformation was obtained, in agreement with the estimated XYN2 pI value (pI = 8.0). This active conformation at pH 8.0 was validated by comparing two independent MD simulations of 100 ps. The following results describe the stability of the XYN2 protein active conformation obtained at pH 8.0.

The MD simulations at pH 8.0 resulted on independent conformational families as depicted by the RMSD trajectory maps (Figure 5). Although the maps clearly indicate a structural convergence of the XYN2 model, the final conformations obtained from both trajectories correspond to slight different local energy minima as revealed by the backbone RMSD. These final stable conformations were ranked as a plausible structural model for the active conformation of the XYN2 protein according to the following criteria: stereo–chemical quality; structural RMSD value for the GH11 family (Table 2); hydrogen network organization; conserved catalytic residues (E84 and E175) (Figure 6B) and the largely conserved residues for stabilization of the 'Thumb" region; pattern of solvent exposed aromatic residues (Figure 4); number of ion pairs and their hydrogen bond network organization. The final model has 111 residues (72.5%), 39 residues (25.5%) and 3 residues (2.0%) in most favorable, allowed and generously regions, respectively, according to Ramachandran plot [24]. The structure of the XYN2 model contains fourteen β–sheet strands classified as antiparallel twisted β–sheet A and B, and one α–helix. Five strands form the antiparallel twisted β–sheet A, whereas generally nine antiparallel strands form the antiparallel twisted β–sheet B. One face of the antiparallel twisted β–sheet B forms a cleft whereas the other one is packed against the antiparallel twisted β–sheet A to form the hydrophobic core [6].

Table 2. The RMS family deviation for the secondary structural arrangement of the retained templates and the final XYN2 model

	BK1	ENX	PVX	UKR	XYN	XYN2	YNA
BK1	0.0	0.95	0.96	0.23	0.90	1.52	1.05
ENX	0.95	0.0	0.69	0.90	0.84	1.21	0.71
PVX	0.96	0.69	0.0	0.94	0.85	1.22	0.37
UKR	0.23	0.90	0.94	0.0	0.87	1.50	1.02
XYN	0.90	0.84	0.85	0.87	0.0	1.44	0.90
XYN2	1.52	1.21	1.22	1.50	1.44	0.0	1.16
YNA	1.05	0.71	0.37	1.02	0.90	1.16	0.0
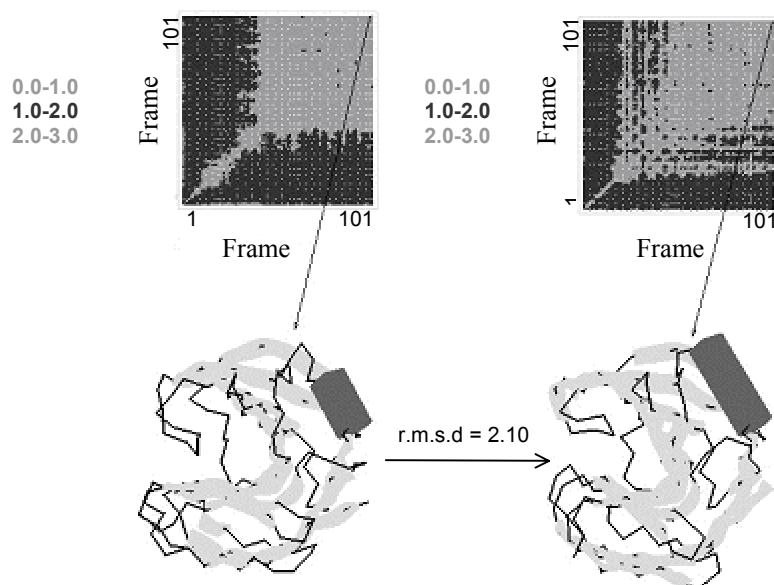
Figure 5. The backbone RMSD clustering map of the conformations, recorded during two independent 100 ps MD simulation in vacuum at pH 8.0. The last frame of each simulation was minimized and is displayed below as a trace with secondary structure. These frames correspond to slight different energy minima, as revealed by the backbone RMSD

As previously reported, aromatic residues within the cleft region are conserved in all of the known xylanase structures and are responsible for binding it to at least four xylose residues, by stacking and hydrogen bonding interactions [36,37]. Indeed, the large cleft of the XYN2 model is occupied by hydrophobic cluster of aromatic residues W17, Y71, Y75, W77, Y86, Y91, and Y94 (Figure 6A). Additionally, many of the conserved proline residues are required for correct folding in the xylanase family. The conserved P96 and P124 are in the *trans*–conformation and P81 is in the *cis*–conformation in the XYN2 model, in agreement with the analyzed templates. The P96 defines the appropriate conformation of the "Cord" region in all the templates [22]. The conserved P124 bends and twists the tip of the thumb region. The P81, belonging to the G76–L82 segment before the signature site 1, which links the B5 and B6 β–strands, configure the active site [36]. Despite structural differences in the "Thumb" and "Cord" regions, the previous analysis of the primary and structural alignment indicated that the overall structure of GH11 family is quite similar. The RMS_Family deviation means score were 0.23 Å and the maximum deviation was 1.52 Å (Table 2).

3.5 Hydrogen Bond Network

In general, the catalytic residues of GH11 family are stabilized by a conserved hydrogen bond network. Conserved aromatic residues such as Tyr and Trp make hydrogen bonds with Glu in signature site 1 whereas an Asn or Asp residue directly stabilizes the Glu of the signature site 2. Figure 6B reveals the arrangement of the catalytic Glu residues of the XYN2 model. E84 and E175 of the XYN2 model are pointed within the cleft by hydrogen bond stabilization. In particular, the catalytic E84 makes hydrogen bonds with Q134, Y86 and Y75. Although the Y75 and W77 are in

T–shape conformation, their side chain can also perform a hydrogen bond.
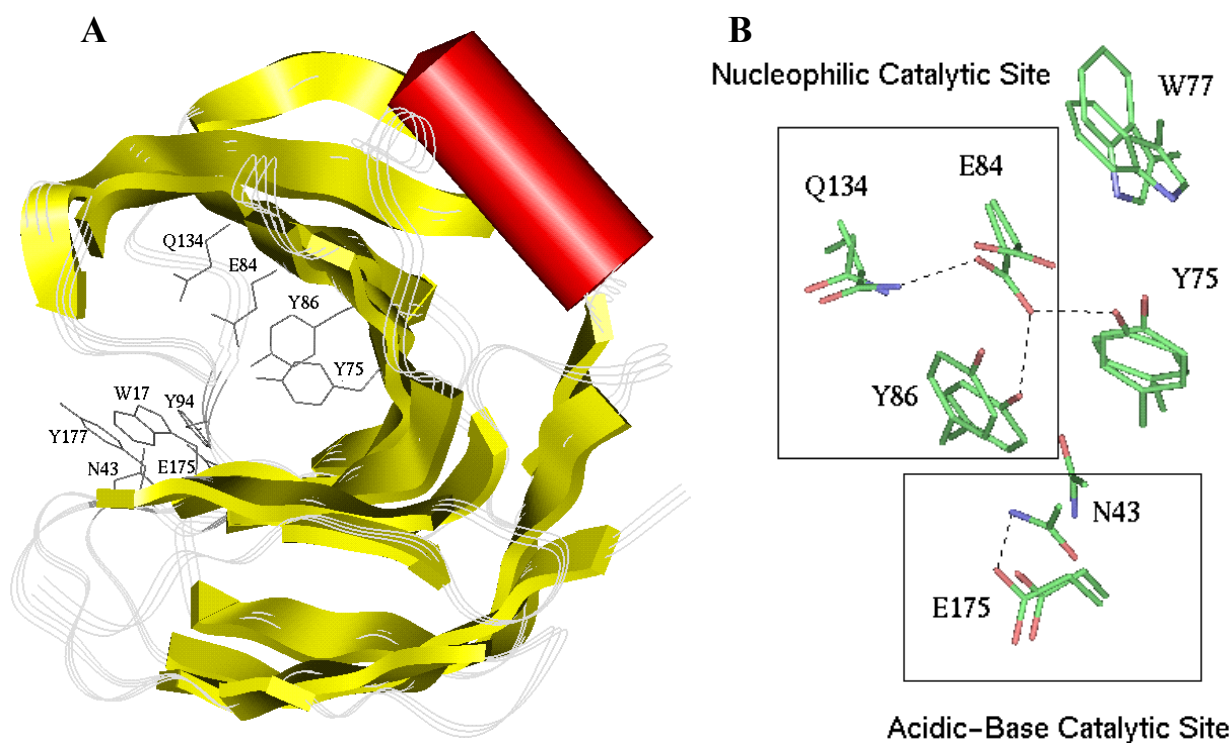
Figure 6. The XYN2 model, and a close–up view of its active site arrangement. **A)** The XYN2 model is represented as strands with secondary structure displayed in yellow and red colors. The trace side chains of the catalytic and hydrophobic cluster residues are pointed to the cleft. **B)** The hydrogen bond network organization of the XYN2 model and 1YNA catalytic site after backbone superimposition.

Asn or Asp interacting with Glu in the signature 2 has been described as a residue to influence critically the xylanase activity on a pH–dependence form [22,36]. In general, enzymes containing Asn have a higher optimum pH than xylanases containing Asp residue at the corresponding position. In that case, the side chain of Asn can serve as hydrogen bond acceptor and hydrogen bond donor as well, and can induce the ionization states of the acid–base catalytic Glu residue in signature 2. Indeed, the catalytic residue E175 is stabilized by N43 residue in the XYN2 model. Additionally, the following residues are conserved in all members of GH11 family [35]: S137, H155, Y113, D109, R139, W157 and E89. These residues constitute the hydrogen–bond network on the XYN2 model. Additionally, the "Thumb" region is stabilized by local hydrophobic interactions and a hydrogen bond network constituted by D127, N80, R79, E6, Y168, S15, T131, N122, Q123, R120, Q133, and T139 residues.

3.6 Effect of pH on Active Site Arrangement

The catalytic mechanism of GH11 family involves two glutamate residues corresponding to E84 (nucleophile) and E175 (acid–base) in the XYN2 sequence [5,38]. The mechanism requires E84 to be unprotonated and E175 to be protonated. In general, the distance between side chains of both

catalytic residues of GH11 family is about 7.0 to 11.0 Å during catalysis [5]. The distance between the two active carboxyl oxygen groups varies depending on the stereo–chemical course of the reaction. The open–close movement of the thumb region was characterized as a "hinge–bending" motion [39]. The catalytic Cα–Cα distances of the XYN2 model are in agreement with all the templates analyzed in this report. Additionally, there is no change in Cα–Cα distances along the MD trajectory (data not shown) suggesting that the active site backbone arrangement showed in the Figure 6B is stable. There is a good agreement between values obtained for the XYN2 model (10.10 Å) and the template used for molecular modeling, 1YNA (10.5 Å).

Most of the known crystal structures of GH11 family adopt the potentially active conformation with short distances (around 7 Å) between the two catalytic Glu residues. Moreover, the distance of 10 Å between carboxylic oxygen atoms of the active Glu residues corresponds to an unfavorable conformation for the substrate access. This side chain displacement between the catalytic residues could reflect functional differences of the enzyme in terms of pH–dependence. Indeed, in many described xylanase proteins the optimum pH is near to the pI [22]. For example, the xylanase from *T. lanuginosus* (YNA) adopts the inactive conformation, which is changed to active conformation in approximately 1.5 pH units away from the optimum pH. Although the GH11 family is a homologous group, a phylogenetic tree has shown distinct xylanase clusters according to alkaline (pI 8–9) and acidic (pI 4–5) pI, in which the pI 8–9 xylanase clusters is most divergent [40].

In the case of XYN2, the overall conformations at pH 7 and pH 8 are different as judged by the backbone RMSD of 2.65 Å. Although the backbone conformation of signature sites 1 and 2 does not depend on the pH (RMSD of 0.99 Å), all atoms superimposition on these regions reveals the dependence of the side chain orientation concerning the pH (RMSD of 2.07 Å). This displacement on the side chain orientation would reflect the difference on the active site hydrogen bond network between the active and inactive conformation. Therefore, it was assumed that the model obtained after 1ns MD run time, at pH 7 (1 pH unit below the pI = 8), adopts the inactive conformation (data not shown) in which the hydrogen bond network is not well configured on the active site. In contrast, the XYN2 model obtained after 100 ps. MD run time, at pH 8, adopts a plausible active conformation in which the two–glutamate catalytic residues were brought closer to defined short distance. Although the active site is sensitive to pH condition, the conformational differences observed could not be completely explained by the ionization states of charged groups, since the total molecular charge at both pH values is +1.

3 CONCLUSIONS

Endo 1,4–β–xylanases are an important group of enzymes with considerable biotechnological applications in paper production and food industries. These processes require an enzyme operating under condition of high temperature and over a broad pH range. Therefore, the thermostability and

pH range for full activity of xylanases are critical properties to design a rational approach to protein engineering. Recently, efforts have been made to improve understanding of the thermostability mechanism of xylanases through analysis of enzymes isolated from thermophilic and mesophilic organisms.

There are various structural factors conferring thermostability of thermophilic xylanases with their mesophilic counterparts. Identified factors are disulfide bonds [41], hydrophobic interactions [37], oligomerization due to solvent exposure of aromatic residues [7], extra–short–range and long range pairs and network organization of charge–charge interactions [35]. Although all these factors may contribute, it seems that the ion–pair interactions, the presence of a disulfide bond and oligomerization are the main factors affecting the thermostability of GH11 family.

In order to understand the structural features, which contribute to the stability of xylanase isolated from *H. grisea* (XYN2), we propose a structural model. The model is in satisfactory agreement with the crystal structures of GH11 family. Additionally, the XYN2 model can provide a structural basis for understanding the role of specific amino acid residues on the thermostability and catalytic activity of xylanases with no disulfide bonds, isolated from thermophilic and mesophilic organisms.

The XYN2 was previously characterized as a thermostable protein [12]. This property was investigated for wild and recombinant XYN2, in *T. reesei* fungus, which was separated in SDS–PAGE 12% gels containing the xylan substrate. The recombinant XYN2 was expressed as a truncated form without 17 amino acid residues in the N–terminal [14]. As reported by deFaria *et al*. [14], the catalytic activity of recombinant XYN2 was reduced up to 50 °C during 30 minutes of incubation, while the wild type preserved the catalytic activity until 70 °C.

One explanation for this experimental result could derive simply from the influence of the 17 N–terminal residues on the stability of the catalytic site. Considering the proposed structural model, an evidence for this assumption comes from the interaction between D18 and N43 of the acidic–basic catalytic site. In this case, the N–terminal localized hydrogen bond network defines the positioning of D18 side chain in order to stabilize N43 by hydrogen bond (data not shown). It is interesting to note that W17 (Figure 6A) is directly involved in the stabilization of the xylan substrate [36,37]. The absence of this side chain would disturb the right positioning of the xylan substrate into the catalytic cleft in order to proceed the enzymatic reaction.

The structural factors contributing to the thermostability of XYN2 were investigated as follow. The relative solvent accessibility and the sequence hydrophobic profile of XYN2 model are similar to both thermophilic (1YNA, 1PVX) and mesophilic (1ENX, 1AXK, 1XYN, 1UKR) templates (Figure 3 and 4). Therefore, the hydrophobic contacts in the XYN2 model could not completely explain the observed thermostability. Additionally, the XYN2 protein does not contain any disulfide bonds, present in many thermophilic xylanases. The thermostability of a xylanase from Bacillus D3

strain was explained by protein oligomerization due the hydrophobic contacts between exposed aromatic residues, known as "sticky patches" interaction [7]. The XYN2 protein has seven solvent exposed aromatic residues (W8, Y63, Y102, Y107, Y121, Y177 and Y186) (Table 3). One "sticky patch" between Y63–Y186 may contribute to, but not fully explain the thermostability of the XYN2 protein.

Table 3. Number of ion pair and exposed aromatic residues

Xylanases	Classification	Number of exposed aromatic residues [a]	Number of ion pair [b]
XYN2	Thermophilic	7	21
1YNA	Thermophilic	1	30
1PVX	Thermophilic	4	18
D3 strain	Thermophilic	11	–
1XYN	Mesophilic	0	12
1BK1	Mesophilic	1	11
1UKRA	Mesophilic	1	14

[a] The aromatic residues were considered exposed above 40% surface exposure.
[b] The electrostatic interactions were analyzed through out of the molecular dynamic concerning the formation of the ion pairs at least 50–fold during the MD simulation. The cut off used was 8 Å.

As has been proposed, the xylanase from *Thermomyces lanuginosus* (1YNA) is a thermostable protein with more sequence and structural similarity with *P. varioti* xylanase (1PVX) than with mesophilic templates [42]. The main structural characteristic is the presence of disulfide bond connecting the thumb to the hinge region in a β–strain B9, including the structural motif of H155–Y115–D111–S139–Water. This motif is conserved on both thermophilic and mesophilic enzymes and also in the XYN2 model. The presence of disulfide bond at the hinge region in thermophilic xylanases can explain in almost GH11 family why thermophilic enzymes are more stable than mesophilic enzyme [42]. Additionally, a comparison of thermophilic with mesophilic families revealed that the disulfide bond and also electrostatic interactions are responsible for the observed thermostability of 1YNA.

The ion pair interactions in the xylanase template and the XYN2 model were calculated using the GROMACS package [43] considering a cut off of 8 Å and using the refined structures from molecular dynamics of 100 ps. run time (see methodology). The numbers of ion pairs are shown in Table 3. Although all the biochemical and structural data are not available to map the physical–chemical properties of the XYN2, the experimental characterized thermostability [14] can be explained by the presence of additional ion pairs and their network organization, comparing to other mesophilic and thermophilic xylanases (Table 3). The XYN2 protein presents twelve negatively charged (6 Asp and 6 Glu) residues and eighteen positively charged (4 Lys, 5 His and 9 Arg) residues. Seven of them are completely conserved on the seven retained templates (Figure 2). Therefore, the XYN2 exhibits 30 charged residues forming 21 ion pair networks. Similarly, among the other thermophilic xylanases, the 1YNA has 35 charged residues forming 30 ion pair

interactions and the 1PVX has 28 charged groups with 18 ion pair interactions. According to our results, the thermostability of the XYN2 protein could be explained by the additional electrostatic network and aromatic exposed residues compared to mesophilic xylanases.

Acknowledgment

5 REFERENCES

[1]   Wilkie, K. C. B. *Adv. Carboh. Chem. Biochem*. **1979**, *36*, 215–264.
[2]   Prade, R. A. *Biotechnol. Genet. Eng. Ver*. **1996**, *13*, 101–131.
[3]   Sunna, A. and Antranikian, G. *Crit. Rev. Biotechnol* **1997**, *17*, 39–67.
[4]   Henrissat, B. and Bairoch, A. *Biochem. J*. **1993**, *293*, 781–788.
[5]   Davies, G. and Henrissat, B. *Structure* **1995**, *3*, 853–859.
[6]   Torronen, A., Harkki, A. and Rouvinen, J. *EMBO J*. **1994**, *13*, 2493–2501.
[7]   Harris, G. W., Pickersgill, R. W., Connerton, I., Debeire, P., Touzel, J. P. and Perez, S. *Proteins* **1997**, *29*, 77–86.
[8]   Viikari, L., Kantelinen, A., Sundquist, J. and Linko, M. *FEMS Microbiol. Rev*. **1994**, *13*, 335–350.
[9]   Jeffries, T. W. *Curr. Opin. Biotechnol*. **1996**, *7*, 337–342.
[10]   De Paula, E. H., Ramos, L. P. and Azevedo, M. O. *Biores. Technol*. **1999**, *68*, 35–41.
[11]   Almeida, E. M., Polizeli, M. L., Jorge, J. A., and Terenzi, H. F. *FEMS Microbiol. Lett*. **1995**, *130*, 171–176.
[12]   Monti, R., Terenzi, H. F. and Jorge, J. A. *Can. J. Microbiol*. **1991**, *37*, 675–681.
[13]   Iikura, H., Takashima, S., Nakamura, A., Masaki, H. and Uozumi, T. *Biosci. Biotech. Biochem*. **1997**, *61*, 1593–1595.
[14]   deFaria, F. P., Teo, V. S. J., Bergquist, P. L., Azevedo, M. O. and Nevalainen, K. M. H. *Lett. Appl. Microbiology* **2002**, *34*, 119–123.
[15]   Araújo, E. F., Barros, E. G., Caldas, R. A. and Silva, D. O. *Biotechnol. Lett*. **1983**, *5*, 781–784.
[16]   Pontecorvo, G., Roper, J., Hemmons, L. H., McDonald and Bufton, W. J. *Adv. Gen*. **1953**, *5*, 141–238.
[17]   Felipe, M. S. S., Rogelin, R., Azevedo, M. O. and Astolfi–Filho, S. *Biotechnol Techniques* **1993**, *7*, 639–644.
[18]   Borges, M. I., Azevedo, M. O., Bonatelli Jr., R., Felipe, M. S. S. and Astolfi–Filho, S. *Fungal Genet. Newslett*. **1990**, *37*, 10.
[19]   Sambrook, J. Fritsch, E. F. and Maniatis, T. **1989**, *Molecular cloning: A laboratory mannual*, 2nd ed. Cold Spring Harbor Laboratory Press, Cold Spring Harbor, NY.
[20]   Altschul, S. F. Stephen, F., Madden, T. L., Schaffer, A. A., Zhang, J., Zhang, Z., Miller, W., and Lipman, D. J. *Nucleic Acids Res*. **1997**, *25*, 3389–3402.
[21]   Pearson, W. R. *Proc Natl Acad Sci USA* **1988**, *85*, 2444–2448.
[22]   Torronen, A. and Rouvinen, J. *J. Biotechnol*. **1997**, *57*, 137–149.
[23]   Shrake, A. and Rupley, J. A. *J. Mol. Biol*. **1973**, *79*, 351–371.
[24]   Laskowiski, R, MacArthur, M. Moss, D. and Thornton, J. *J. Appl. Crystallogr*. **1993**, *26*, 283–290.
[25]   Dalboege, H. and Heldt–Hansen, H. P. *Mol. Gen. Genet*. **1994**, *243*, 253–260.
[26]   Kinoshita, K., Takano, M., Koseki, T., Ito, K. and Iwano, K. *J. Ferment. Bioeng*. **1995**, *79*, 422–428.
[27]   Kitamoto, N., Yoshino, S., Ito, M., Kimura, T., Ohmiya, K. and Tsukagoshi, N. *Appl. Microbiol. Biotechnol*. **1998**, *50*, 558–563.
[28]   Cubero, B. and Scazzocchio, C. *EMBO J*. **1994**, *13*, 407–415.
[29]   Apel, P. C., Panaccione, D. G.; Holden, F. R. and Walton, J. D. *Mol. Plant. Microbe Interact*. **1993**, *6*, 467–473.
[30]   Perez–Gonzalez, J. A., De Graaff, L. H., Visser, J. and Ramon, D. *Appl. Environ. Microbiol*. **1996**, *62*, 2179–82.
[31]   Ito, K., Iwashita, K. and Iwano, K. *Biosci. Biotechnol. Biochem*. **1992**, *56*, 1338–1340.
[32]   Törrönen, A., Mach, R. L., Messner, R., Gonzalez, R., Kalkkinen, N., Harkki, A. and Kubicek, C. P. *Biotechnol*. **1992**, *10*, 1461–1465.
[33]   Gavel, Y. and von Heijne, G. *Prot. Engin*. **1990**, *3*, 433–442.
[34]   Henrissat, B. and Bairoch, A. *Biochem. J*. **1996**, *316*, 695–696.
[35]   Gruber, K., Klinstchar, G., Hayn, M., Schlacher, A., Steiner, W. and Kratky, C. *Biochem*. **1998**, *37*, 13475–13485.
[36]   Krengel, U. and Dijkstra, B. W. *J. Mol. Biol*. **1996**, *263*, 70–78.
[37]   Connerton, I., Cummings, N., Harris, G. W., Debeire, P. and Breton, C. *Biochim. Biophys. Acta* **1999**, *1433*, 110–121.

[38] Biely, P., Vrsanská, M. Tenkanen, M. and Kluepfel, D. *J. Biotechnology* **1997**, *57*, 151–166.
[39] Muilu, J., Torronen, A., Perakyla, M. and Rouvinen, J. *Protein* **1998**, *31*, 434–444.
[40] Torronen, A., Kubicek, C. P. and Henrissat, B. *FEBS Lett*. **1993**, *321*, 135–139.
[41] Wakarchuk, W. W., Sung, W. L., Campbell, R. L., Cunningham, A., Watson, D. C. and Yaguchi, M. *Protein Eng*. **1994**, *7*, 1379–1386.
[42] Kumar, P. R., Eswaramoorthy, S., Vithayathil, P. J. and Viswamitra, M. A. *J. Mol. Biol*. **2000**, *295*, 581–593.
[43] Van der Spoel, D., van Buuren, A. R., Apol, E., Meulenhoff, P. J., Tieleman, D. P., Sijbers, A. L. T. M., Hess, B., Feenstra, K. A., Lindahl, E., van Drunen, R. and Berendsen, H. J. C. **1999**. Gromacs User Manual version 2.0. Nijenborgh 4, 9747 AG Groningen, The Netherlands. (http://md.chem.rug.nl/~gmx).
[44] Torronen, A. and Rouvinen, J. *Biochem*. **1995**, *34*, 847–856.
[45] Ay, J., Gotz, F., Borriss, R. and Heinemann, U. *Proc. Natl. Acad. Sci. USA* **1998**, *95*, 6613–6618.
[46] Eswaramoorthy, S., Vithayathil, P. J. and Viswamitra, M. A. *J. Mol. Biol*. **1994**, *243*, 806–808.
[47] Fushinobu, S., Ito, K., Konno, M., Wakagi, T. and Matsuzawa, H. *Protein Eng*. **1998**, *11*, 1121–1128.

Biographies

Sonia M. De Freitas is professor of Cellular Biology Department at the University of Brasília. Dr. Freitas undertook research of protein structure in collaboration with crystallography group from Laboratório Nacional de Luz Sincrotron (LNLS) – Campinas, Brazil

This work is *in memorian* of Dr. **Maristella O**. **Azevedo**. She was a professor of Cellular Biology at the University of Brasília, in the Molecular Biology Laboratory. She had worked for twenty years with hydrolytic enzymes, especially with lignocellulolytic enzymes from the fungus *Humicola grisea* var. *thermoidea*. She isolated the genes from the cellulolytic and xylanolytic system with the aim of studying these enzymes and their biotechnological applications. Dr Azevedo was an important scientific leader and a special colleague who was admired for both professional and personal qualities. We hope all the people that knew Maristella could learn from her ideals as a scientific and human being.